

Time-Varying Graph Learning with Constraints on Graph Temporal Variation

Haruki Yokota, *Student Member, IEEE*, Koki Yamada, *Member, IEEE*, Yuichi Tanaka, *Senior Member, IEEE*,
and Antonio Ortega, *Fellow, IEEE*

Abstract—We propose a novel framework for learning time-varying graphs from spatiotemporal measurements. Given an appropriate prior on the temporal behavior of signals, our proposed method can estimate time-varying graphs from a small number of available measurements. To achieve this, we introduce three regularization terms in convex optimization problems that constrain the sparseness of temporal variations of the time-varying networks. Moreover, a computationally scalable algorithm is introduced to solve the optimization problem efficiently. The experimental results with synthetic and real datasets (point cloud, temperature, and EEG data) demonstrate that our proposed method outperforms state-of-the-art methods.

Index Terms—Graph learning, time-varying graph, topology identification, network inference, dynamic graph.

I. INTRODUCTION

SIGNALS often have underlying network structures, e.g., in sensor, traffic, brain, and social networks. Graphs, consisting of sets of nodes and edges, are fundamental tools for describing the relationship among entities. Graph edges and the corresponding edge weights can capture the similarity between nodes (where a higher positive weight indicates greater similarity). Introducing a graph representation enables us to efficiently analyze signals on networks in many practical applications, such as epidemics [1], [2], transportation networks [3], and social networks [4].

Even when data is not associated with an actual network, graphs are efficient tools to represent latent structures in the data. For example, a principal component analysis can be improved by imposing a prior based on graphs [5]–[7]. Graph-based image processing enables us to improve performance in several image processing tasks [8]–[13]. However, graphs are often not known *a priori*.

Graph learning methods aim at identifying graphs from observed data [14]–[20]. Each observation is a vector, with each entry in the vector corresponding to an observation at one node. The goal of graph learning is to obtain the weights of all the edges connecting those nodes. Most graph learning methods identify a single static graph from all the observations

[21]–[32]. These *static graph learning* methods assume that the node relationships obtained from the observations do not change during the measurement process.

In many applications, observations are obtained over a period of time, and a time-varying (TV) graph can provide a better model. Examples of such applications include estimation of the time-varying brain functional connectivity from EEG or fMRI data [33], identification of temporal transit of biological networks such as protein, RNA, and DNA [34], inference of relationships among companies from historical stock price data [35], dynamic point cloud processing, and analysis of sensor network data.

A straightforward approach to estimating a TV graph consists of aggregating temporal observations into non-overlapping windows and then using an existing static graph learning method to estimate a graph for each time window. However, such an approach has some drawbacks. First, this method estimates a graph *independently* for each temporal interval; thus, it ignores temporal relations that may exist in TV graphs. Second, time-varying graph learning may require estimating graphs from time windows containing only a small fraction of observations, given the trade-off between the choice of window length and temporal resolution. Specifically, if we choose a short window to adapt to fast temporal graph changes, we may not have enough data to learn a graph within each window since existing static graph learning methods cannot successfully infer graphs from a small number of observations. On the other hand, if we use a larger window, we may be unable to track relatively fast temporal changes.

This paper presents a *time-varying graph learning* method based on time-varying graph factor analysis (TGFA), which is an extension of its static counterpart, static graph factor analysis (SGFA) [22]. We propose TGFA-based methods to estimate TV graphs from a collection of spatiotemporal measurements. SGFA assumes a signal generation model based on a graph signal processing (GSP) perspective, with the observed signals having specific spectral properties with respect to the graph Fourier transform (GFT) of the graph to be learned. For example, under a multivariate Gaussian model, we assume that observed signals are generated from a Gaussian distribution whose inverse covariance matrix is given by the graph Laplacian of the underlying graph [14], [22]. Unlike SGFA, TGFA considers the graph evolution, which is represented by a sequence of graph Laplacians as illustrated in Fig. 1.

This study focuses on three separate TV graph models, each corresponding to one of the following properties:

1) **Temporal homogeneity (TH)**: We assume that most

H. Yokota and K. Yamada contributed equally to this work.

H. Yokota and Y. Tanaka are with the Graduate School of Engineering, The University of Osaka, Osaka 565-0871, Japan (e-mail: h.yokota@sip.comm.eng.osaka-u.ac.jp and ytanaka@comm.eng.osaka-u.ac.jp).

K. Yamada is with the Graduate School of Engineering, Tokyo University of Agriculture and Technology, Tokyo 184-8588, Japan (e-mail: k-yamada@go.tuat.ac.jp).

A. Ortega is with the Department of Electrical and Computer Engineering, University of Southern California, Los Angeles, CA 90089 USA (aortega@usc.edu).

TABLE I
COMPARISON OF GRAPH LEARNING METHODS

Setting	Author	Model	Memory	Target Graphs	Regularization	Processing	Bidirectional
Time-varying	Proposed	Smoothness	$1-L$	$2-T$	Multiple	Batch	Yes
	Yamada et al. [36]	Smoothness	1	$2-T$	L1	Batch	No
	Kalofolias et al. [37]	Smoothness	1	$2-T$	Tikhonov	Batch	No
	Hallac et al. [35]	Graphical	1	$2-T$	Multiple	Batch / Streaming	No
	Zhang et al. [38]	Smoothness	$1-T-1$	$2-T$	L1	Batch	Yes
	Ye et al. [39]	Smoothness	1	$2-T$	L2	Batch	No
Online	Natali et al. [40]	Multiple	1	1	-	Streaming	No
	Bagheri et al. [41]	Stationarity	1	1	Low-rank	Batch	No
Multiple	Saboksayr et al. [42]	Smoothness	1	C	-	Batch / Streaming	-
	Rey et al. [43]	Stationarity	1	C	L1	Batch	-

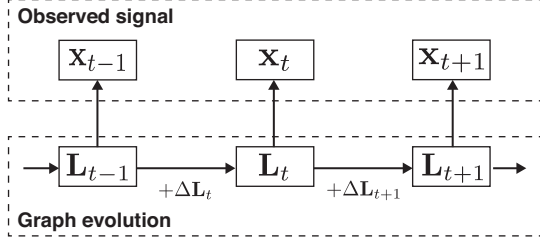


Fig. 1. An overview of TV graph factor analysis. \mathbf{L}_t and $\Delta\mathbf{L}_t$ represent the graph Laplacian at the t th time slot and the graph temporal variation. This study focuses on learning a TV graph, which is the sequence of the graph Laplacian, from the observed signal \mathbf{x} .

edges and their weights in the TV graph model remain unchanged over a short-term time horizon, i.e., only a few graph edges change at any given time. TV graphs in many applications satisfy this property. For example, consider a sensor network where the nodes represent sensor locations. Often, the edges are chosen to capture information about correlations among sensor measurements. If the sensors record the temperature in a building, various factors, such as air conditioning, sunlight, and the number of people in the room, locally affect the correlations among the sensor measurements. However, these factors vary smoothly over time. As a result, data on this sensor network can be modeled by a TV graph where the connectivity itself does not change frequently, but the edge weights can change smoothly over time. TV graphs in fMRI and various biological networks can also be seen as having this property [34], [44].

2) Switching behavior (SB): We assume both edges and weights remain unchanged most of the time; however, they may change within a few time slots. This model reflects sudden changes in graph topologies. Prominent examples include brain networks, where epileptic seizures can lead to sudden changes in graph model topology [45].

3) Local topological changes (LTC): We assume that most edges and weights remain unchanged over time, while the connectivity of a small portion of nodes changes for each time slot. An example of this behavior can be seen in mobile sensor networks, where some sensors may relocate themselves over time to form a different local neighborhood [46].

In this paper, we design an algorithm to estimate these three types of TV graphs with a consistent objective function. For this purpose, we formulate the graph learning problem as a convex optimization with regularization of temporal variation

TABLE II
LIST OF NOTATION

N	Number of nodes
E	Number of edges
K	Number of data chunk
T	Number of time frames
L	Number of temporal filter taps
$a_i, (\mathbf{a})_i, a[i]$	i th entry of a vector
$A_{ij}, (\mathbf{A})_{ij}$	(i, j) entry of a matrix
$(\mathbf{A})_i$	i th column of \mathbf{A}
\mathbf{A}^\dagger	Moore-Penrose pseudoinverse of \mathbf{A}
\circ	Hadamard product
$\ \mathbf{a}\ _2^2, \ \mathbf{A}\ _F^2$	Sum of squared values of all elements
$\ \mathbf{a}\ _1, \ \mathbf{A}\ _1$	Sum of absolute values of all elements
$\ \mathbf{A}\ _{2,1} = \sum_i \ (\mathbf{A})_i\ _2$	
$\text{Tr}(\mathbf{A})$	Trace of a matrix
$\text{diag}(\mathbf{A})$	Vector formed by diagonal elements

derived from TGFA. To solve the convex optimization problem, we utilize a primal-dual splitting algorithm [47], which enables us to estimate TV graphs more successfully than static graph learning methods. Furthermore, while the model shown in Fig. 1 is a *single-step memory* model where learning a new graph includes a constraint based on the most recently learned graph, it is also possible to consider *multi-step memory* cases where the constraints are based on the previous L learned graphs. We show that our formulation can be easily adapted to such L -step memory cases.

In experiments with synthetic datasets, our proposed method outperforms existing methods, especially when only small amounts of data are available. We also evaluate the performance of our methods for tasks involving real data. Our results for dynamic point cloud denoising show that estimating graph topology information with our method allows us to improve the denoising performance. In a meteorological and temperature data application, we show that our method can learn reasonable TV graphs that capture the geographical characteristics *without using geographical information*. In an experiment with electroencephalogram (EEG) data, the graphs learned from EEGs of epileptic seizures with our method can illustrate the structural variance during the seizure, which is consistent with clinical observations.

Our published preliminary work [36] proposed a TV graph learning framework for **TH** under the single-step memory setting. In our preprint [48], we introduced the **SB** model and proposed a solution. This paper includes the **TH** model

from our peer-reviewed publication [36], and extends it with an updated version of the **SB** model from [48] and the newly introduced **LTC** model along with the L -step memory case. We also propose a new unified methodology to formulate and solve all three problems and evaluate our approach under different conditions through extensive experiments on synthetic and real-world datasets, comparing its computational complexity with competing approaches.

A. Related Works

Recent overviews of graph learning are given in [14], [15]. Typical approaches for learning TV graphs solve problems that consist of two terms, one quantifying the smoothness of signals on the graph and another that provides regularization to characterize graph evolution over time.

Many approaches, including our method, assume (spatial) signal smoothness on the TV graphs. The key difference between the methods lies in the choice of the regularization terms. In [37], the smoothness of edge weights between adjacent time windows is considered in an ℓ_2 sense, using Tikhonov regularization. In [38], total variation regularization is applied to capture sparse changes between pairs of time-varying graphs. However, the optimization proposed in [37] lacks the flexibility for other types of temporal changes, such as **TH**, and the model in [38] requires prior knowledge about how the graphs evolve. In contrast, we demonstrate that our algorithm is suited for learning TV graphs with the properties **TH**, **SB**, and **LTC** and can accommodate other models.

The TV graph learning method in [35] uses TV graphical Lasso, which combines graphical Lasso with a temporal regularization and finds the solution using the alternating direction method of multipliers (ADMM). Note that graphs estimated with this approach often have negative edge weights. In contrast, our proposed method is constrained to have non-negative edges in the estimated graph, which are often desired for many applications [14], [15]. Furthermore, our method has a lower computation complexity: TV graphical Lasso requires eigendecompositions of target matrices to calculate a proximal operator of a logarithm determinant term, whereas our approach is eigendecomposition-free.

The problem of identifying a TV graph to capture causal relationships in the evolution of network contagion has been studied in prior work [35]. This model focuses on the spread process on networks (e.g., infectious diseases and fake news) and aims to identify the links propagating information over nodes at each time. However, only directed graphs can be estimated by this approach. In contrast, our method estimates undirected graphs whose connections change over time. This is often desired for data that do not have causal relationships, such as data acquired by physical sensors (e.g., point cloud coordinates and temperature readings).

The above-mentioned models, including ours, are *offline* approaches that compute a set of TV graphs from the observed data. Conversely, several *online* TV graph learning methods have been proposed in recent research. For example, [41] proposes a joint graph learning and signal interpolation method that assumes low-rank temporal variation, updating the graph

at t based on the one at $t-1$. Other online methods [40], [42] also follow this sequential approach. We provide a summary of state-of-the-art TV graph learning methods in Table I.

The remainder of this paper is organized as follows. Section II presents preliminaries about graphs and proximal operators. Section III introduces the problem formulation of time-varying graph learning. Section IV defines regularization terms for temporal graph variation and the corresponding graph learning optimization problem, and proposes an algorithm to find a solution. Section V and Section VI provide experimental results with synthetic and real data, respectively. Finally, the conclusions and future work are presented in Section VII.

II. PRELIMINARIES

The notation used in this paper is summarized in Table II. Vectors and matrices are written in bold lowercase and uppercase letters, respectively. The calligraphic capital letters, namely, \mathcal{V} and \mathcal{W}_m , denote sets. $\mathcal{O}(\cdot)$ and $\Omega(\cdot)$ are the big-O and big-Omega notations used in complexity theory.

A. Basic GSP Definitions

An undirected weighted graph is represented as $\mathcal{G} = (\mathcal{V}, \mathcal{E}, \mathbf{W})$, where \mathcal{V} is a set of nodes, $\mathcal{E} = \{(i, j)\}_{i, j \in \mathcal{V}}$ is a set of edges, and \mathbf{W} is a weighted adjacency matrix. The number of nodes is given by $N = |\mathcal{V}|$, and the number of edges is given by $E = |\mathcal{E}| \leq N(N-1)/2$. Each element of the weighted adjacency matrix is defined by

$$(\mathbf{W})_{mn} = \begin{cases} w_{mn} & \text{if nodes } m \text{ and } n \text{ are connected,} \\ 0 & \text{otherwise,} \end{cases} \quad (1)$$

where $w_{mn} \geq 0$ is the edge weight between nodes m and n . The degree matrix \mathbf{D} is a diagonal matrix whose diagonal element is $d_{mm} = \sum_n w_{mn}$. The graph Laplacian is given by $\mathbf{L} = \mathbf{D} - \mathbf{W}$. Let $\mathbf{f} \in \mathbb{R}^N$ be a signal on the graph, then the Laplacian quadratic form is given by

$$\mathbf{f}^\top \mathbf{L} \mathbf{f} = \frac{1}{2} \sum_{m,n} w_{mn} (f_m - f_n)^2, \quad (2)$$

where f_m and f_n denote the signal values at nodes m and n , respectively. Note that (2) provides a measure to quantify the smoothness of \mathbf{f} [49], [50].

Because \mathbf{L} is a real symmetric matrix, it has orthogonal eigenvectors and can be decomposed into $\mathbf{L} = \mathbf{U} \mathbf{\Lambda} \mathbf{U}^\top$, where $\mathbf{U} = [\mathbf{u}_0, \mathbf{u}_1, \dots, \mathbf{u}_{N-1}]$ is a matrix whose i -th column is the eigenvector \mathbf{u}_i and $\mathbf{\Lambda} = \text{diag}(\lambda_0, \lambda_1, \dots, \lambda_{N-1})$ is a diagonal eigenvalue matrix. The graph Fourier transform (GFT) is defined as: $\hat{f}[i] = \langle \mathbf{u}_i, \mathbf{f} \rangle = \sum_{n=0}^{N-1} u_i[n] f[n]$. Eigenvalues of the graph Laplacian correspond to frequencies in the classical Fourier transform and, thus, are often called *graph frequencies*.

B. Proximal Operator and Its Properties

Let $f : \mathbb{R}^n \rightarrow \mathbb{R} \cup \{\infty\}$ be a proper lower semicontinuous convex function. The proximal operator $\text{prox}_{\gamma f} : \mathbb{R}^n \rightarrow \mathbb{R}^n$ of f with a parameter $\gamma > 0$ is defined by

$$\text{prox}_{\gamma f}(\mathbf{x}) = \arg \min_{\mathbf{y}} f(\mathbf{y}) + \frac{1}{2\gamma} \|\mathbf{y} - \mathbf{x}\|_2^2. \quad (3)$$

If a proximal operator $\text{prox}_{\gamma f}$ can be computed efficiently, the function f is called proximal.

Proximal operators have the following properties [51]:

- If a function f is separable across variables, i.e., $f(\mathbf{x}) = f_1(\mathbf{x}_1) + f_2(\mathbf{x}_2)$ with $\mathbf{x} = [\mathbf{x}_1^\top \mathbf{x}_2^\top]^\top$, then

$$\text{prox}_{\gamma f}(\mathbf{x}) = [(\text{prox}_{\gamma f_1}(\mathbf{x}_1))^\top (\text{prox}_{\gamma f_2}(\mathbf{x}_2))^\top]^\top, \quad (4)$$

where $\mathbf{x} = [\mathbf{x}_1^\top \mathbf{x}_2^\top]^\top$. Thus, the computation in the proximal operator of separable functions reduces to the computation of the proximal operator for each separable part.

- If a function f is fully separable, i.e., $f(\mathbf{x}) = \sum_i f_i(x_i)$, then

$$(\text{prox}_{\gamma f}(\mathbf{x}))_i = \text{prox}_{\gamma f_i}(x_i). \quad (5)$$

Therefore, in this case, the computation of the proximal operator can be reduced to the element-wise computation.

III. STATIC AND TIME-VARYING GRAPH FACTOR ANALYSIS

We first describe SGFA [22], which introduces a model for the generation of graph signals. Subsequently, we introduce TGFA, which extends SGFA to formulate the time-varying graph learning problems studied in this paper.

A. Static Graph Factor Analysis (SGFA)

The observation model of SGFA is defined [22]:

$$\mathbf{x} = \mathbf{U}\mathbf{h} + \epsilon, \quad (6)$$

where $\mathbf{x} \in \mathbb{R}^N$ is an observed signal, $\mathbf{h} \in \mathbb{R}^N$ is a latent variable represented in the graph frequency domain, \mathbf{U} is the GFT matrix and $\epsilon \sim \mathcal{N}(0, \sigma_\epsilon^2 \mathbf{I})$ is an additive white Gaussian noise. From (6), signals can be represented by the inverse GFT of latent variables in the spectral domain of the underlying graph. SGFA assumes that the latent variable \mathbf{h} follows the multivariate Gaussian distribution

$$p(\mathbf{h}) = \mathcal{N}(0, \mathbf{\Lambda}^\dagger). \quad (7)$$

This corresponds to the assumption that signal energy tends to be concentrated in the low frequencies and thus encourages graph signal smoothness. (6) and (7) lead to the conditional probability of \mathbf{x} given \mathbf{h} :

$$p(\mathbf{x}|\mathbf{h}) = \mathcal{N}(\mathbf{U}\mathbf{h}, \sigma_\epsilon^2 \mathbf{I}). \quad (8)$$

From (7) and (8), the marginal distribution of \mathbf{x} is given by:

$$p(\mathbf{x}) = \mathcal{N}(0, \mathbf{L}^\dagger + \sigma_\epsilon^2 \mathbf{I}). \quad (9)$$

Note that the fact $\mathbf{L}^\dagger = \mathbf{U}\mathbf{\Lambda}^\dagger\mathbf{U}^\top$ is used in the derivation of (9). The marginal distribution in (9) indicates that a graph signal \mathbf{x} can be generated by the degenerate multivariate Gaussian distribution whose precision matrix is the graph Laplacian of the underlying graph. Signals generated from the distribution (9) satisfy graph stationarity [52] because their covariance and graph Laplacian are jointly diagonalizable by the eigenvectors of the graph Laplacian. The maximum a posteriori estimation of \mathbf{h} leads to the following problem [22]:

$$\min_{\mathbf{L}, \mathbf{y}} \|\mathbf{x} - \mathbf{y}\|_2^2 + \alpha \mathbf{y}^\top \mathbf{L} \mathbf{y}, \quad (10)$$

where $\mathbf{y} = \mathbf{U}\mathbf{h}$ and \mathbf{y} is regarded as a noiseless signal. This problem is solved by an optimization that alternates denoising and graph learning steps [22]. However, this optimization cannot guarantee the convergence to the optimal solution in general. To avoid this, by assuming $\mathbf{y} = \mathbf{x}$, (10) is reformulated as the problem of finding the graph Laplacian that minimizes the smoothness measure $\mathbf{x}^\top \mathbf{L} \mathbf{x}$ under some constraints [21], [27], [37].

B. Time-varying Graph Factor Analysis (TGFA)

Suppose that we have a multivariate time series data divided into non-overlapping time windows¹ $\{\mathbf{X}_1, \dots, \mathbf{X}_T\}$, where $\mathbf{X}_t = [\mathbf{x}_1^{(t)}, \dots, \mathbf{x}_K^{(t)}] \in \mathbb{R}^{N \times K}$ contains the K observations corresponding to time window t , and the graph corresponding to observations within a time window is invariant. Our goal is to learn a sequence of graph Laplacians $\mathbf{L}_1, \dots, \mathbf{L}_T$, where \mathbf{L}_t corresponds to \mathbf{X}_t .

We extend SGFA by incorporating a graph evolution process, so TFGA is defined as:

$$\mathbf{x}^{(t)} \sim \mathcal{N}(0, \mathbf{L}_t^\dagger + \sigma_\epsilon^2 \mathbf{I}), \quad (11)$$

$$\mathbf{L}_t = \begin{cases} \mathbf{0} & t = 0 \\ \mathbf{L}_{t-1} + \Delta \mathbf{L}_t & t \geq 1, \end{cases} \quad (12)$$

where $\mathbf{x}^{(t)}$, \mathbf{L}_t , and $\Delta \mathbf{L}_t$ are a signal, the graph Laplacian of the underlying graph and a graph update, representing the graph variation at a given time t , respectively. The probability distribution of $\mathbf{x}^{(t)}$ in (11) indicates that time-varying graph learning requires the TV observations to be smooth on the corresponding learned graphs. Introducing $\Delta \mathbf{L}_t$ in (12) allows us to incorporate prior knowledge about temporal graph variation.

Given the TGFA, a time-varying graph learning problem consists of estimating a set of graph Laplacians minimizing $\sum_t \mathbf{x}^{(t)\top} \mathbf{L}_t \mathbf{x}^{(t)}$. The temporal graph variation is thus controlled by regularization term(s) corresponding to $\Delta \mathbf{L}_t$.

The generalized time-varying graph learning problem leads to the following optimization:

$$\min_{\mathbf{L}_t \in \mathcal{L}} \sum_{t=1}^T \text{Tr}(\mathbf{X}_t^\top \mathbf{L}_t \mathbf{X}_t) + f(\mathbf{L}_t) + \eta \sum_{t=2}^T R(\Delta \mathbf{L}_t \circ \mathbf{H}), \quad (13)$$

where \mathcal{L} is the valid set of graph Laplacians and is given by

$$\mathcal{L} = \{ \mathbf{L} \in \mathbb{R}^{N \times N} \mid \mathbf{L} = \mathbf{L}^\top, L_{ij} \leq 0 \ (i \neq j), \\ L_{ii} = - \sum_{j \neq i} L_{ij} \}, \quad (14)$$

in which $\mathbf{H} = \mathbf{1}\mathbf{1}^\top - \mathbf{I}$. In (13), $R(\Delta \mathbf{L}_t \circ \mathbf{H})$ is a regularization term that characterizes the temporal change in graph edges, that is, the off-diagonal elements of the temporal graph variation $\Delta \mathbf{L}_t$. The first term in (13) corresponds to the smoothness term in the static case (10) and quantifies the smoothness of the signals on TV graphs. The function in the second term $f(\mathbf{L}_t)$ is a regularization to avoid obtaining trivial solutions. This function, examples of which will be given later, depends on the assumptions made about the graph model. The parameter η controls the regularization strength.

¹With slight modifications, overlapping sliding windows can also be used.

We first focus on the single-step memory case formulation, where $\Delta \mathbf{L} := \mathbf{L}_t - \mathbf{L}_{t-1}$. The same approach can be applied for the multi-step memory case by replacing $\Delta \mathbf{L}$ in (13) by a function involving multiple \mathbf{L}_t (see Section IV-C).

To obtain a tractable formulation with simplified conditions for the valid set, we reformulate the problem (13) with constraint (14) by using weighted adjacency matrices instead of graph Laplacians. This leads to a problem equivalent to that of (13):

$$\min_{\mathbf{W}_t \in \mathcal{W}_m} \sum_{t=1}^T \frac{1}{2} \|\mathbf{W}_t \circ \mathbf{Z}_t\|_1 + f(\mathbf{W}_t) + \eta \sum_{t=2}^T R(\mathbf{W}_t - \mathbf{W}_{t-1}), \quad (15)$$

where the valid set of weighted adjacency matrices is

$$\mathcal{W}_m = \{\mathbf{W} \in \mathbb{R}_+^{N \times N} \mid \mathbf{W} = \mathbf{W}^\top, W_{ii} = 0\}. \quad (16)$$

The first term of (15) is equal to $\text{Tr}(\mathbf{X}_t^\top \mathbf{L}_t \mathbf{X}_t)$, since [21]:

$$\text{Tr}(\mathbf{X}_t^\top \mathbf{L}_t \mathbf{X}_t) = \frac{1}{2} \text{Tr}(\mathbf{W}_t \mathbf{Z}_t) = \frac{1}{2} \|\mathbf{W}_t \circ \mathbf{Z}_t\|_1, \quad (17)$$

where \mathbf{Z}_t is the pairwise distance matrix defined by $(\mathbf{Z}_t)_{ij} = \sum_{k=1}^K \|(\mathbf{x}_k^{(t)})_i - (\mathbf{x}_k^{(t)})_j\|^2$.

In this paper, we solve the optimization problem in (15) to learn a TV graph. Throughout this paper, we set the regularization for the weighted adjacency matrix to be [37]:

$$f(\mathbf{W}_t) = -\alpha \mathbf{1}^\top \log(\mathbf{W}_t \mathbf{1}) + \beta \|\mathbf{W}_t\|_F^2, \quad (18)$$

where α and β are the parameters. The first term in (18) forces the degree on each node to be positive without preventing edge weights from becoming zero. The second term controls the magnitude of edge weights.

For learning TV graphs, the graph temporal variation term $R(\cdot)$ should be chosen appropriately. In [37], a temporal variation regularizer $R(\cdot) = \|\cdot\|_F^2$ is selected to learn TV graphs such that the edge weights change smoothly over time. In the next section, we describe the regularization terms to learn TV graphs with models **TH**, **SB**, and **LTC**, followed by the methods to solve the optimization problem.

IV. LEARNING TV GRAPH WITH TEMPORAL VARIATION REGULARIZATION

Specific regularization terms for graph temporal variation should be chosen based on the type of temporal graph evolution suitable for a given application. In this paper, we consider three types of graph evolution terms, which appear in many applications, and present an algorithm to solve the corresponding optimizations.

A. Formulation

1) **Temporal Homogeneity (TH)**: In the first model, we assume that most edges and their weights will likely remain unchanged over a short-term time horizon. Thus, as the regularizer $R(\cdot)$ in (15), we aim to minimize the ℓ_1 norm

of the adjacency matrices between the time slots t and $t-1$. This leads to the following *fused Lasso* formulation [53]:

$$\min_{\mathbf{W}_t \in \mathcal{W}_m} \sum_{t=1}^T \frac{1}{2} \|\mathbf{W}_t \circ \mathbf{Z}_t\|_1 + f(\mathbf{W}_t) + \eta \sum_{t=2}^T \|\mathbf{W}_t - \mathbf{W}_{t-1}\|_1. \quad (19)$$

To make the optimization problem tractable, we rewrite (19) in vector form, with \mathbf{W}_t and \mathbf{Z}_t replaced by $\mathbf{w}_t \in \mathbb{R}_+^{N(N-1)/2}$ and $\mathbf{z}_t \in \mathbb{R}_+^{N(N-1)/2}$ respectively. Only the upper-triangular parts of \mathbf{W}_t and \mathbf{Z}_t are considered, given that the graph is undirected.

Let us define $\mathbf{w} = [\mathbf{w}_1^\top \mathbf{w}_2^\top \dots \mathbf{w}_T^\top]^\top$, $\mathbf{z} = [\mathbf{z}_1^\top \mathbf{z}_2^\top \dots \mathbf{z}_T^\top]^\top$, and $\mathbf{d} = [\mathbf{d}_1^\top \mathbf{d}_2^\top \dots \mathbf{d}_T^\top]^\top$ where $\mathbf{d}_t = \mathbf{W}_t \mathbf{1}$. We also introduce the linear operators \mathbf{S} and Φ that satisfy $\mathbf{S}\mathbf{w} = \mathbf{d}$ and $\Phi\mathbf{w} = \mathbf{w} - \hat{\mathbf{w}}$ respectively, where $\hat{\mathbf{w}} = [\mathbf{w}_1^\top \mathbf{w}_1^\top \mathbf{w}_2^\top \dots \mathbf{w}_{T-1}^\top]^\top$. Then, we can rewrite (19) and (18) as

$$\min_{\mathbf{w} \in \mathcal{W}_v} \mathbf{z}^\top \mathbf{w} - \alpha \mathbf{1}^\top \log(\mathbf{S}\mathbf{w}) + \beta \|\mathbf{w}\|_2^2 + \eta \|\Phi\mathbf{w}\|_1, \quad (20)$$

where

$$\mathcal{W}_v = \{\mathbf{w} \in \mathbb{R}^{TN(N-1)/2} \mid w_i \geq 0 \ (i = 1, 2, \dots)\} \quad (21)$$

represents the non-negativity constraint. The symmetric and diagonal constraints can be simplified by expressing (16) in vector form.

2) **Switching Behavior (SB)**: The second model aims to learn graphs with switching behavior. In this case, the graphs remain almost constant for most time slots, but are allowed to undergo sudden changes at a few time slots. To reflect this characteristic, we consider the Frobenius norm of the differences between the adjacency matrices at t and $t-1$, i.e., $\|\mathbf{W}_t - \mathbf{W}_{t-1}\|_F$. To maintain this term small, the TV graphs should be almost static over time. The resulting optimization problem is:

$$\min_{\mathbf{W}_t \in \mathcal{W}_m} \sum_{t=1}^T \frac{1}{2} \|\mathbf{W}_t \circ \mathbf{Z}_t\|_1 + f(\mathbf{W}_t) + \eta \sum_{t=2}^T \|\mathbf{W}_t - \mathbf{W}_{t-1}\|_F, \quad (22)$$

where only the last term differs from (19), allowing more edge weights to change, while changes remain infrequent.

To make the optimization problem tractable, we rewrite (22) in the same manner as in the previous model as:

$$\min_{\mathbf{w} \in \mathcal{W}_v} \mathbf{z}^\top \mathbf{w} - \alpha \mathbf{1}^\top \log(\mathbf{S}\mathbf{w}) + \beta \|\mathbf{w}\|_2^2 + \eta \sum_j \|\Phi\mathbf{w}\|_j, \quad (23)$$

where $[\Phi\mathbf{w}]_j = \mathbf{w}_j^\top - \mathbf{w}_{j-1}^\top$, $j = 2, \dots, T$.

3) **Local Topological Changes (LTC)**: In the third model, we assume that the connectivity is nearly static, but local changes are possible. That is, for a few nodes, several connections will change, while for most nodes, at most one connection change will occur. At each time, the set of nodes changing can be different. Mathematically, when this happens, the matrix of changes $\mathbf{W}_t - \mathbf{W}_{t-1}$ will exhibit row sparsity (only a few rows will contain non-zero entries), which can be characterized by the matrix $\ell_{2,1}$ -norm regularization [54]. Thus, we consider the following formulation for LTC:

$$\min_{\mathbf{W}_t \in \mathcal{W}_m} \sum_{t=1}^T \frac{1}{2} \|\mathbf{W}_t \circ \mathbf{Z}_t\|_1 + f(\mathbf{W}_t) + \eta \sum_{t=2}^T \|\mathbf{W}_t - \mathbf{W}_{t-1}\|_{2,1}. \quad (24)$$

The $\ell_{2,1}$ norm is also known as *group Lasso* [55]. Let us consider a case of a *concentrated* change in an unweighted graph, where a node changes its connection with M nodes. In this case, the $\ell_{2,1}$ norm penalty will be $M + \sqrt{M}$, while the Frobenius norm penalty will be $\sqrt{2M}$. In contrast, if all these changes are *distributed*, e.g., two nodes each change their connection with $M/2$ distinct nodes (no overlap between the two sets of newly connected or disconnected neighbors), the $\ell_{2,1}$ norm penalty will be $M + \sqrt{M/2}$ while the Frobenius norm penalty will be the same as the previous case. This indicates that the Frobenius norm regularization is insensitive to the structure of the change, while the $\ell_{2,1}$ norm regularization encourages the model to learn structurally sparse solutions. To make the optimization problem tractable, we rewrite (24) in the same manner as the previous model:

$$\min_{\mathbf{w} \in \mathcal{W}_v} \mathbf{z}^\top \mathbf{w} - \alpha \mathbf{1}^\top \log(\mathbf{S}\mathbf{w}) + \beta \|\mathbf{w}\|_2^2 + \eta \sum_j \sum_i \|[\Phi \mathbf{w}]_j^{(i)}\|_2, \quad (25)$$

where $[\Phi \mathbf{w}]_j^{(i)} = [\mathbf{w}_j^\top - \mathbf{w}_{j-1}^\top]^{(i)}$, $i = 1, \dots, N, j = 2, \dots, T$. $[\Phi \mathbf{w}]_j^{(i)}$ represents a vector whose elements are i -th row of the temporal variation of the adjacency matrix.

B. Optimization

Since the proposed regularization terms are not differentiable, these optimization problems cannot be solved directly using the methods in [37]. Thus, we solve (20), (23) and (25) with a primal-dual splitting (PDS) method [47], which solves a problem in the form,

$$\min_{\mathbf{w}} f_1(\mathbf{w}) + f_2(\mathbf{w}) + f_3(\mathbf{M}\mathbf{w}), \quad (26)$$

where f_1 is a differentiable convex function with gradient ∇f_1 and Lipschitz constant ξ ; f_2 and f_3 are proper lower semi-continuous convex functions which are proximal; and \mathbf{M} is a linear operator.

Many algorithms to solve (26) have been proposed [47], [56], [57]. We use a forward-backward-forward (FBF) approach [58], which allows parallel computation of the proximal operators of f_2 and f_3 .

1) *Temporal Homogeneity (TGL-TH)*: By introducing the indicator function of \mathcal{W}_v in (21), we rewrite (20) as follows:

$$\min_{\mathbf{w}} \mathbf{z}^\top \mathbf{w} - \alpha \mathbf{1}^\top \log(\mathbf{S}\mathbf{w}) + \beta \|\mathbf{w}\|_2^2 + \eta \|\Phi \mathbf{w}\|_1 + \iota_{\mathcal{W}_v}(\mathbf{w}), \quad (27)$$

where the indicator function $\iota_{\mathcal{W}_v}$ is defined by

$$\iota_{\mathcal{W}_v}(\mathbf{w}) = \begin{cases} 0 & w_i \geq 0 \\ \infty & \text{otherwise.} \end{cases} \quad (28)$$

The objective function (27) further reduces to the applicable form of the PDS as follows:

$$\begin{aligned} f_1(\mathbf{w}) &= \beta \|\mathbf{w}\|_2^2 \quad \text{with } \xi = 2\beta, \\ f_2(\mathbf{w}) &= \mathbf{z}^\top \mathbf{w} + \iota_{\mathcal{W}_v}(\mathbf{w}), \\ f_3(\mathbf{v}) &= -\alpha \mathbf{1}^\top \log(\mathbf{v}_1) + \eta \|\mathbf{v}_2\|_1, \\ \mathbf{M} &= \begin{bmatrix} \mathbf{S} \\ \Phi \end{bmatrix}, \end{aligned} \quad (29)$$

where the dual variable is $\mathbf{v} := \mathbf{M}\mathbf{w} = [\mathbf{v}_1^\top \mathbf{v}_2^\top]^\top$.

The proximal operator of f_2 is given by

$$(\text{prox}_{\gamma(\|\cdot\|_1 + \iota_{\mathcal{W}_v})}(\mathbf{x}))_i = \begin{cases} 0 & x_i \leq \gamma \\ x_i - \gamma & \text{otherwise.} \end{cases} \quad (30)$$

Because f_3 is separable across variables, the proximal operator can be computed separately for each term (see (4)). The proximal operator for the log barrier function [51] as the first term of f_3 is given by

$$(\text{prox}_{\gamma(-\mathbf{1}^\top \log(\cdot))}(\mathbf{x}))_i = \frac{x_i + \sqrt{x_i^2 + 4\gamma}}{2}. \quad (31)$$

The proximal operator for the ℓ_1 -norm, i.e., the second term in f_3 , is well known to be the element-wise soft-thresholding operation [51]:

$$(\text{prox}_{\gamma\|\cdot\|_1}(\mathbf{x}))_i = \begin{cases} 0 & |x_i| \leq \gamma \\ \text{sgn}(x_i)(|x_i| - \gamma) & \text{otherwise.} \end{cases} \quad (32)$$

See Algorithm 1 for the complete algorithm.

2) *Switching Behavior (TGL-SB) and LTC (TGL-LTC)*: The objective functions (23) and (25) for **SB** and **LTC**, respectively, can be reduced to the PDS applicable form similar to the first model. For (23), we can replace f_3 with

$$f_3(\mathbf{v}) = -\alpha \mathbf{1}^\top \log(\mathbf{v}_1) + \eta \sum_{j=2}^T \|[\mathbf{v}_2]_j\|_2, \quad (33)$$

where $[\mathbf{v}_2]_j = [\Phi \mathbf{w}]_j$.

For (25), we can replace f_3 with

$$f_3(\mathbf{v}) = -\alpha \mathbf{1}^\top \log(\mathbf{v}_1) + \eta \sum_{j=2}^T \sum_{i=1}^N \|[\mathbf{v}_2]_j^{(i)}\|_2, \quad (34)$$

where N is the number of nodes and $[(\mathbf{v}_2)]_i^{(i)} = [\Phi \mathbf{w}]_i^{(i)}$.

The proximal operator of the second term in the equations above is the block-wise soft-thresholding operation [51]:

$$\text{prox}_{\gamma\|\cdot\|_2}([\mathbf{x}]_j) = \begin{cases} \mathbf{0} & \|\mathbf{x}\|_2 \leq \gamma \\ (1 - \gamma/\|\mathbf{x}\|_2)([\mathbf{x}]_j) & \text{otherwise.} \end{cases} \quad (35)$$

Because the proximal operator of the functions f_2 and f_3 can be computed efficiently, the second model can also be solved with the PDS algorithm.

Algorithm 1 summarizes the above solvers. The hyperparameter γ in the PDS algorithm is determined such that the convergence condition [56] is satisfied. Since our proposed optimization problem is convex and lower-semicontinuous, algorithm convergence is guaranteed.

C. Extension to L-step Memory Cases

In the model proposed in (15), we define the temporal variation of the graph as a difference in edge weights in two consecutive time windows, $\mathbf{W}_t - \mathbf{W}_{t-1}$. The temporal difference operator $\Phi \in \mathbb{R}^{ET \times ET}$ thus needs to satisfy

$$\Phi \mathbf{w} = \begin{bmatrix} \mathbf{w}_1 - \mathbf{w}_1 \\ \mathbf{w}_2 - \mathbf{w}_1 \\ \vdots \\ \mathbf{w}_T - \mathbf{w}_{T-1} \end{bmatrix}. \quad (36)$$

TABLE III
LIST OF ALTERNATIVE AND PROPOSED METHODS

	Method	Approach	Temporal Regularization	Computational Complexity
Static	SGL-Glasso [23]	Graphical Lasso based model	-	$\mathcal{O}(T(N^2 + \Omega(N^3)))$
	SGL-Smooth [21]	Signal smoothness model	-	$\mathcal{O}(TN^2)$
TV	TGL-Tik [37]	Signal smoothness + Regularization	$\sum_{t=2}^T \ \mathbf{W}_t - \mathbf{W}_{t-1}\ _F^2$	$\mathcal{O}(TN^2)$
	TGL-TH (proposed)	Signal smoothness + Regularization	$\sum_{t=2}^T \ \mathbf{W}_t - \mathbf{W}_{t-1}\ _1$	$\mathcal{O}(TN^2)$
	TGL-SB (proposed)	Signal smoothness + Regularization	$\sum_{t=2}^T \ \mathbf{W}_t - \mathbf{W}_{t-1}\ _F$	$\mathcal{O}(TN^2)$
	TGL-LTC (proposed)	Signal smoothness + Regularization	$\sum_{t=2}^T \ \mathbf{W}_t - \mathbf{W}_{t-1}\ _{2,1}$	$\mathcal{O}(TN^3)$

Algorithm 1 Proposed PDS Algorithm Solver

Input: $\mathbf{w}^{(0)}, \mathbf{v}_1^{(0)}, \mathbf{v}_2^{(0)}$
Output: $\mathbf{w}^{(i)}$

while $\|\mathbf{w}^{(i+1)} - \mathbf{w}^{(i)}\| / \|\mathbf{w}^{(i)}\| > \epsilon$ **do**
 $\mathbf{y}^{(i)} = \mathbf{w}^{(i)} - \gamma(2\beta\mathbf{w}^{(i)} + \mathbf{S}^\top \mathbf{v}_1^{(i)} + \Phi^\top \mathbf{v}_2^{(i)})$
 $\bar{\mathbf{y}}_1^{(i)} = \mathbf{v}_1^{(i)} + \gamma(\mathbf{S}\mathbf{w}^{(i)})$
 $\bar{\mathbf{y}}_2^{(i)} = \mathbf{v}_2^{(i)} + \gamma(\Phi\mathbf{w}^{(i)})$
 $\mathbf{p}^{(i)} = \text{prox}_{\gamma(\|\cdot\|_1 + \iota_{\mathcal{W}_v})}(\mathbf{y}^{(i)})$
 $\bar{\mathbf{p}}_1^{(i)} = \bar{\mathbf{y}}_1^{(i)} - \gamma \text{prox}_{\frac{1}{\gamma}}(-\mathbf{1}^\top \log(\cdot))\left(\frac{\bar{\mathbf{y}}_1^{(i)}}{\gamma}\right)$
 $\bar{\mathbf{p}}_2^{(i)} = \begin{cases} \bar{\mathbf{y}}_2^{(i)} - \gamma \text{prox}_{\frac{1}{\gamma}\|\cdot\|_1}\left(\frac{\bar{\mathbf{y}}_2^{(i)}}{\gamma}\right) & \text{to solve (20)} \\ \bar{\mathbf{y}}_2^{(i)} - \gamma \text{prox}_{\frac{1}{\gamma}\|\cdot\|_2}\left(\frac{\bar{\mathbf{y}}_2^{(i)}}{\gamma}\right) & \text{to solve (23) and (25)} \end{cases}$
 $\mathbf{q}^{(i)} = \mathbf{p}^{(i)} - \gamma(2\beta\mathbf{p}^{(i)} + \mathbf{S}^\top \bar{\mathbf{p}}_1^{(i)} + \Phi^\top \bar{\mathbf{p}}_2^{(i)})$
 $\bar{\mathbf{q}}_1^{(i)} = \bar{\mathbf{p}}_1^{(i)} + \gamma(\mathbf{S}\mathbf{p}^{(i)})$
 $\bar{\mathbf{q}}_2^{(i)} = \bar{\mathbf{p}}_2^{(i)} + \gamma(\Phi\mathbf{p}^{(i)})$
 $\mathbf{w}^{(i+1)} = \mathbf{w}^{(i)} - \mathbf{y}^{(i)} + \mathbf{q}^{(i)}$
 $\mathbf{v}_1^{(i+1)} = \mathbf{v}_1^{(i)} - \bar{\mathbf{y}}_1^{(i)} + \bar{\mathbf{q}}_1^{(i)}$
 $\mathbf{v}_2^{(i+1)} = \mathbf{v}_2^{(i)} - \bar{\mathbf{y}}_2^{(i)} + \bar{\mathbf{q}}_2^{(i)}$
end while

As a result, Φ is defined as:

$$\Phi = \begin{bmatrix} \mathbf{0}_E & \mathbf{0}_E & \mathbf{0}_E & & \mathbf{0}_E \\ -\mathbf{I}_E & \mathbf{I}_E & \mathbf{0}_E & \dots & \mathbf{0}_E \\ \mathbf{0}_E & -\mathbf{I}_E & \mathbf{I}_E & & \mathbf{0}_E \\ & \vdots & & \ddots & \\ \mathbf{0}_E & \mathbf{0}_E & \mathbf{0}_E & -\mathbf{I}_E & \mathbf{I}_E \end{bmatrix}, \quad (37)$$

which is the first-order difference of the time-varying edge weights.

The choice of Φ reflects an assumption about the expected type of time-varying behavior. Other Φ can be chosen to extend these ideas to the L -step memory setting for $L \geq 2$. For example, Φ for $L = 2$ is defined as:

$$\Phi = \begin{bmatrix} \mathbf{0}_E & \mathbf{0}_E & \mathbf{0}_E & & \mathbf{0}_E \\ \mathbf{0}_E & \mathbf{0}_E & \mathbf{0}_E & \dots & \mathbf{0}_E \\ -\mathbf{I}_E & -\mathbf{I}_E & 2\mathbf{I}_E & & \mathbf{0}_E \\ & \vdots & & \ddots & \\ \mathbf{0}_E & \mathbf{0}_E & -\mathbf{I}_E & -\mathbf{I}_E & 2\mathbf{I}_E \end{bmatrix}, \quad (38)$$

For $L = 2$, we can also define Φ as a cyclic operator

$$\Phi = \begin{bmatrix} 2\mathbf{I}_E & -\mathbf{I}_E & \mathbf{0}_E & & -\mathbf{I}_E \\ -\mathbf{I}_E & 2\mathbf{I}_E & -\mathbf{I}_E & \dots & \mathbf{0}_E \\ \mathbf{0}_E & -\mathbf{I}_E & 2\mathbf{I}_E & & \mathbf{0}_E \\ & \vdots & & \ddots & -\mathbf{I}_E \\ -\mathbf{I}_E & \mathbf{0}_E & \mathbf{0}_E & -\mathbf{I}_E & 2\mathbf{I}_E \end{bmatrix}, \quad (39)$$

which is a bidirectional prediction of time-varying graphs. Note that we can further parameterize the coefficient on each time slot, creating a trade-off between flexibility and computational efficiency. Also, L can be set to be any number as long as $L \leq T - 1$. Note that increasing the memory size will lead to a more static temporal behavior.

The L -step memory setting can also be found in a TV graph where the graph alternates between two states, such as dense to sparse, with some probability over time [59]. In this case, we could design a TV graph learning problem with an appropriate Φ by connecting the time slots in the same/similar state. We can also design Φ to take the difference of adjacency matrices among several time slots according to a (pre-defined) temporal connectivity as in [38]. We compare the performance of the standard first-order temporal model, which only penalizes the deviations from the previous time step ($L = 1$), against models incorporating longer-range dependencies, specifically with memory length of $L = 2$ and $L = 3$ in Section V-C.

Defining a “good” design of Φ or the optimal choice of the memory length L generally depends on the application and would require prior knowledge about the characteristics of the temporal evolution of the graph. Therefore, it is beyond the scope of this paper and is left for future work.

D. Computational Complexity

In Table III, we summarize the computational complexities of representative graph learning methods. We compare static graph learning (SGL) methods, including graphical lasso (SGL-Glasso) [23] and smoothness prior (SGL-Smooth) [21], to time-varying graph learning (TGL) such as Tikhonov regularization (TGL-Tik) [37], to our three proposed approaches: temporal homogeneity regularization (TGL-TH), switching behavior regularization (TGL-SB), and local topological changes regularization (TGL-LTC).

SGL-Glasso updates each row/column of the graph Laplacian at each time slot by solving non-negative quadratic programming, which requires at least N^3 order of computation. Therefore the computational complexity for SGL-Glasso is

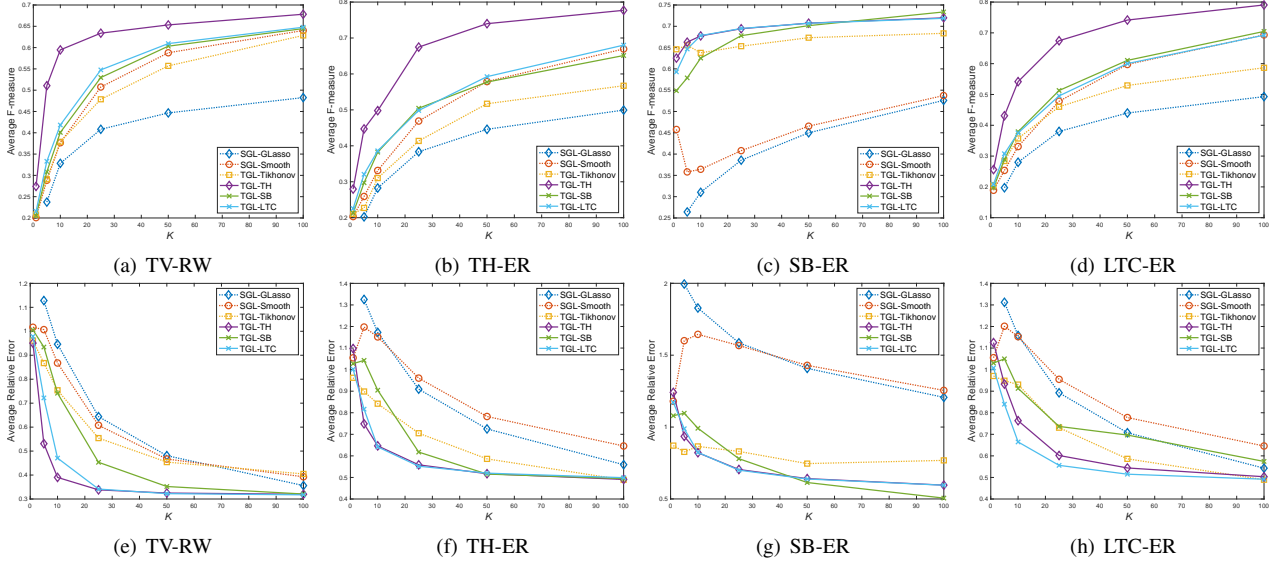


Fig. 2. The performance of learning TV graphs for different numbers of data samples. The top row demonstrates the F-measure for the datasets based on TV-RW graph, TH-ER graph, SB-ER graph, and LTC-ER graph, respectively. The bottom row demonstrates the relative error for those datasets.

$\mathcal{O}(T(N^2 + \Omega(N^3)))$ per iteration. For SGL-Smooth, the upper triangular components of the adjacency matrix are updated per time slot, which leads to the complexity $\mathcal{O}(TN^2)$ per iteration.

The computational complexity of the TV graph learning algorithms mainly depends on the computation of the proximity operators (e.g., (31) and (35)). For TGL-Tik and the first two of our learning problems (TGL-TH and TGL-SB), the complexity is $\mathcal{O}(TN^2)$ per iteration. The third model (TGL-LTC) computes the proximity operator N times more, resulting in the complexity of $\mathcal{O}(TN^3)$ per iteration. As observed from Table III, most methods (except SGL-Glasso and TGL-LTC) have the same order of computational complexity.

V. EXPERIMENTAL RESULTS WITH SYNTHETIC DATASET

The proposed TGL methods are performed on synthetic data in this section. First, the details of datasets and performance metrics are shown, and then the accuracies of graph learning methods are compared.

A. Synthetic Datasets

We construct datasets in two steps: 1) building TV graphs, and 2) generating signals from a probability distribution based on the graph Laplacians of the created TV graph. Four types of synthetic graphs are considered: 1) a TV graph based on the random waypoint model (abbreviated as TV-RW graph) [60], 2) a temporal homogeneity-based Erdős-Rényi graph (TH-ER graph), 3) a switching behavior-based ER graph (SB-ER graph), and 4) an LTC-based ER graph (LTC-ER graph). Each TV-graph is created with $N = 36$ nodes for 300 time slots. The details of the four TV graphs are as follows:

- 1) TV-RW: TV graphs with smooth edge variation. A 3-nearest-neighbor graph was constructed based on the simulated movement of 36 sensors in a square space, with positions sampled over time.
- 2) TH-ER: TV graphs with sparse edge variation. An initial ER graph was generated with edge connection

probability $p = 0.05$, and at each subsequent time step, 5% of the edges were resampled.

- 3) SB-ER: TV graphs with infrequent, sudden changes. Six different static ER graphs were created with $p = 0.50$. Starting from a random initial state at $t = 1$, the graph at each time slot had a 5% probability of switching to a different state.
- 4) LTC-ER: Localized, frequent connectivity changes. An initial ER graph was created with $p = 0.30$. At each time step, 5% of the nodes had their connectivity recomputed, while the rest of the graph remained stationary.

The edge weights for TV-RW are determined based on the Euclidean distance d_{ij} between nodes i and j as $W_{ij} = \exp(-d_{ij}/2\theta)$ where θ is a parameter. The edge weights for TH-ER, SB-ER, and LTC-ER are set to be uniformly distributed in the interval $[0, 1]$.

Using the graph Laplacian \mathbf{L}_t at time t , a data sample \mathbf{x}_t is generated from a Gaussian Markov random field model

$$p(\mathbf{x}_t | \mathbf{L}^{(t)}) = \mathcal{N}(\mathbf{x}_t | 0, \mathbf{L}_t^\dagger + \sigma^2 \mathbf{I}), \quad (40)$$

where σ^2 is the covariance of the Gaussian noise. We set $\sigma = 0.5$ in this experiment. Samples generated with (40) have close signal values when two nodes are connected.

B. Performance Comparison

1) *Experimental Conditions:* We evaluate the performance in terms of relative error and F-measure, each averaged over all the time slots. The relative error is given by

$$\text{Relative error} = \frac{\|\widehat{\mathbf{W}} - \mathbf{W}^*\|_F}{\|\mathbf{W}^*\|_F}, \quad (41)$$

where $\widehat{\mathbf{W}}$ is the estimated weighted adjacency matrix, and \mathbf{W}^* is the ground truth. It reflects the accuracy of edge weights on the estimated graph. The F-measure is given by

$$\text{F-measure} = \frac{2tp}{2tp + fn + fp}, \quad (42)$$

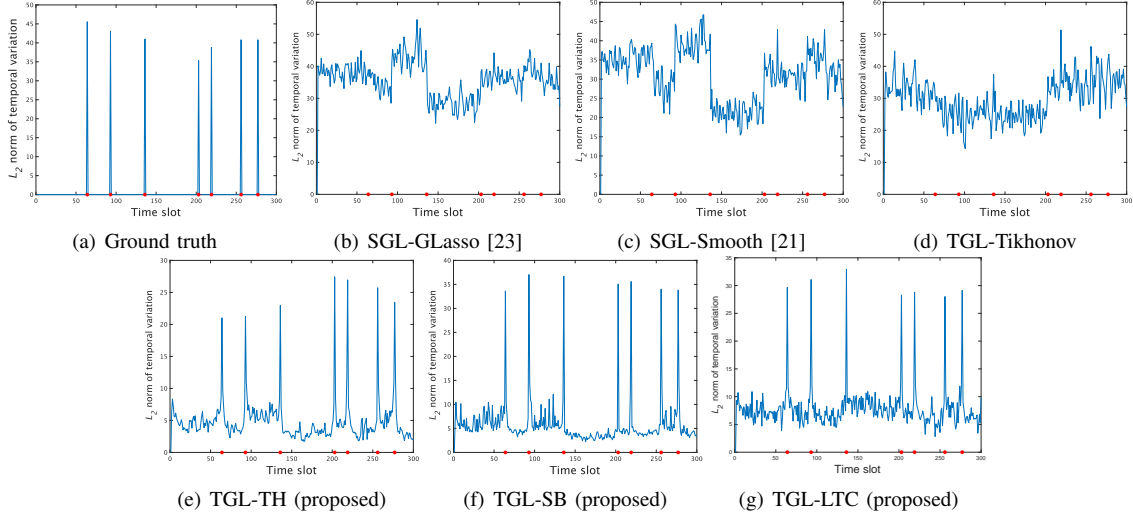


Fig. 3. The visualization of the temporal variations in the TV graph learned from the dataset based on the graph in which large fluctuations occur at a few time slots. Red points in these figures represent time slots where the connectivity state changes.

where the true positive (tp) is the number of edges that are included both in $\widehat{\mathbf{W}}$ and \mathbf{W}^* , the false positive (fp) is the number of edges that are not included in $\widehat{\mathbf{W}}$ but are included in \mathbf{W}^* , and the false negative (fn) is the number of edges that are included in $\widehat{\mathbf{W}}$ but are not included in \mathbf{W}^* . The F-measure, the harmonic average of the precision and recall, represents the accuracy of the estimated graph topology and takes values between 0 and 1. The higher the F-measure is, the higher the performance of capturing the graph topology is.

We perform Monte-Carlo simulations for each method to find the parameters minimizing the relative error. Note that, as shown in the next section, fixed parameters still work well for our graph learning with real-world data. For SGL-Smooth, TGL-Tik, and the proposed methods, α is selected by fine-tuning, and β is fixed to $\beta = 0.05$. The parameter η for all TGL methods is selected from 0.1 to 2 in steps of 0.1 to achieve the best relative error. The parameter for SGL-GLasso is selected by the method described in [23]. The tolerance value ϵ in Algorithm 1 is set to 1.0×10^{-3} . We evaluate the performance of each method using different data sample sizes, $K = \{1, 5, 10, 25, 50, 100\}$, and measure the average relative error and F-measure for each sample size across 10 independent trials. Note that SGL-GLasso is not evaluated with $K = 1$ because the sample covariance used in SGL-GLasso cannot be calculated.

2) *Results*: As shown in Fig. 2, our proposed time-varying (TV) graph learning methods outperform static approaches and the TGL-Tik baseline (Figs. 2(a), 2(e)). Each method demonstrated strength in specific scenarios: TGL-TH's ℓ_1 regularization worked well for graphs with smooth/sparse variations like TH-ER and LTC-ER (Figs. 2(a), 2(d)); TGL-SB was most effective for the sudden, infrequent changes of the SB-ER graph, especially with more observations ($K \geq 50$) (Figs. 2(c), 2(g)); and TGL-LTC showed robust, flexible performance across many models, especially when changes were localized as in the LTC-ER graph (Figs. 2(e), 2(f), 2(h)).

In addition, Fig. 3 shows the L_2 -norm of the temporal difference of learned adjacency matrices in each time slot, i.e.,

$\|\mathbf{W}_t - \mathbf{W}_{t-1}\|_2$. Clearly, TGL-TH, TGL-SB, and TGL-LTC can detect sudden changes in the graph in time slots, while SGL-GLasso and SGL-Smooth have several unclear jumps. On the other hand, TGL-Tik can suppress the temporal variation of graphs better than SGL-Smooth, but it obscures the change points in the TV graph. As a result, the proposed TGL methods are suitable for change detection.

C. Effect of Memory Size L

To verify the effect of memory size L , mentioned in Section IV-C, we perform TV graph learning for the TV-RW graph with perturbation on edge weights. That is, data samples \mathbf{x}_t is generated by (40) but from the following *noisy* edge weights:

$$\tilde{W}_{ij} = \begin{cases} W_{ij} + \epsilon & \text{if } W_{ij} + \epsilon > 0 \\ 0 & \text{otherwise} \end{cases} \quad (43)$$

where $\epsilon \sim \mathcal{N}(0, 0.1^2)$. We set $K = 5$ and compare the average relative error and F-measure of 50 independent runs. We set $L = \{1, 2, 3\}$. Note that $L = 1$ is the baseline that only considers the relationship to the immediate previous adjacency matrix \mathbf{W}_{t-1} . The temporal variation operator Φ for the proposed algorithm with $L \in \{2, 3\}$ is defined in (38). For comparison, we extend the TGL-Tik [37] by generalizing its temporal regularizer $\sum_{t=2}^T \|\mathbf{W}_t - \mathbf{W}_{t-1}\|_F^2$, shown in Table III, for any memory length L by:

$$\sum_{l=1}^L \sum_{t=l+1}^T \|\mathbf{W}_t - \mathbf{W}_{t-l}\|_F^2. \quad (44)$$

We apply this formulation for $L \in \{2, 3\}$ in our experiments.

The results presented in Table IV show a consistent performance increase for all TGL algorithms as L grows. This implies that the robustness against the noise induced to edge weights in (43) is improved by increasing the memory size L , as long as the edge weights vary smoothly over time.

TABLE IV
RELATIVE ERROR (RE) AND F-MEASURE (FM) WITH DIFFERENT MEMORY LENGTH

Method	SGL-smooth		TGL-Tik		TGL-LTC		TGL-TH		TGL-SB	
Metric	RE	FM	RE	FM	RE	FM	RE	FM	RE	FM
Static	0.898	0.459	-	-	-	-	-	-	-	-
$L = 1$	-	-	0.715	0.515	0.550	0.523	0.491	0.591	0.768	0.493
$L = 2$	-	-	0.677	0.523	0.423	0.551	0.416	0.634	0.687	0.511
$L = 3$	-	-	0.664	0.524	0.392	0.560	0.409	0.654	0.613	0.525

TABLE V
DENOISING RESULTS: SNR (dB)

Method	<i>dog</i>	<i>handstand</i>	<i>skirt</i>	<i>wheel</i>
noisy	12.12	13.97	13.73	15.45
k -NN	12.35	14.29	14.01	15.76
SGL-Smooth	13.13	15.37	15.03	16.74
TGL-Tik	13.34	15.69	15.34	17.06
TGL-TH	20.05	21.32	21.58	22.97

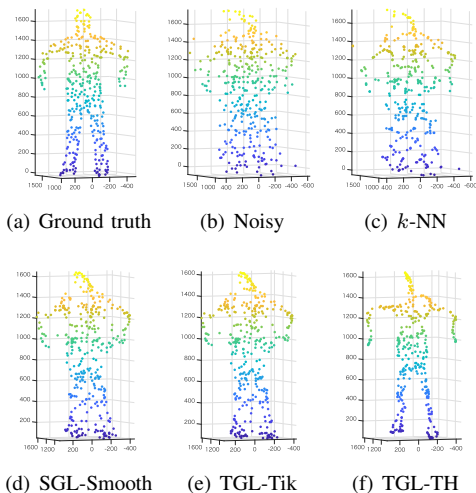


Fig. 4. The visualization of denoising result of *wheel* at a $t = 10$ time.

VI. EXPERIMENTS WITH REAL-WORLD DATA

A. Dynamic Point Clouds

We apply our method for dynamic point cloud (DPC) data denoising. DPC data contain 3D coordinates of dynamically evolving points. Graphs for point cloud data are typically constructed using static methods such as kNN graphs. However, when point cloud data are acquired, it is often contaminated

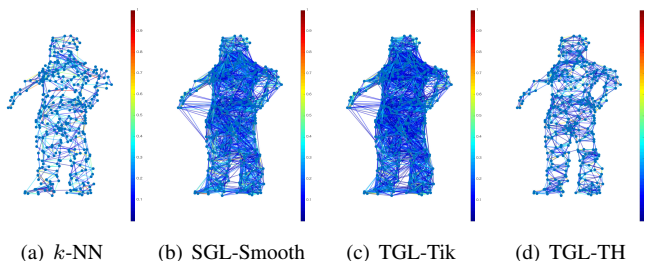


Fig. 5. The visualization of a graph at a certain time in the TV graph learned from the noisy point cloud data.

with noise due to measurement errors, which leads to displacements of the geometric coordinates of the point clouds. Therefore, considering the temporal difference of graphs is expected to enhance noise removal performance. We use graph heat kernel filtering [61] for denoising. The TV graph used in the denoising is estimated from noisy point cloud data.

We use the DPC dataset in [62], which contains five DPCs: *dance*, *dog*, *handstand*, *skirt*, and *wheel*. As this dataset is clean data, with position ranges from -260 to 1932 , we added Gaussian noise with $\sigma = 90$, a very high noise level. The TV graph is learned from the dataset downsampled to 357 points and evolving over 240 time slots. In this experiment, we use fixed parameters for each method, which are determined by a grid search with *dance* data, and evaluate the denoising performance with the other four data.

Table V summarizes our DPC denoising results. We observe that the TV graph learning methods perform better than SGL-Smooth and k -nearest neighbor (k -NN), indicating that the k -NN fails to construct a meaningful graph from noisy data. Additionally, TGL-TH outperformed TGL-Tik by up to 6 dB.

Fig. 4 shows the visualization of denoising results of the *wheel* at a certain time. Similar to the numerical performance, the k -NN cannot capture the structure of the human body. SGL-Smooth and TGL-Tik yield slightly better outputs than those by the k -NN; however, the arms and legs are still problematic. On the other hand, TGL-TH can better capture the structure of the human body than the other methods.

Fig. 5 visualizes a graph at time slot $t = 10$ in the TV graph estimated from the noisy *wheel* data in the dynamic point cloud dataset. In this figure, the nodes in the graphs are plotted in the correct position for visualization. As shown in the figure, the k -NN method yields a sparse graph, but the edge weights and the connectivity are directly affected by noise. In Fig. 5(a), we can observe heavily (lightly) weighted edges between nodes that are far apart (close by), especially between the left and the right legs. SGL-Smooth and TGL-Tik yielded very dense edges and connected different parts of the body. In contrast, TGL-TH yields graphs whose connectivity preserves the human body structure.

B. Temperature Data

We also apply the proposed method to estimate a TV graph from temperature data on the island of Hokkaido, the northernmost region in Japan. The goal of this experiment is to learn a TV graph to explore the relationship between geographical regions over time. In this experiment, we use the

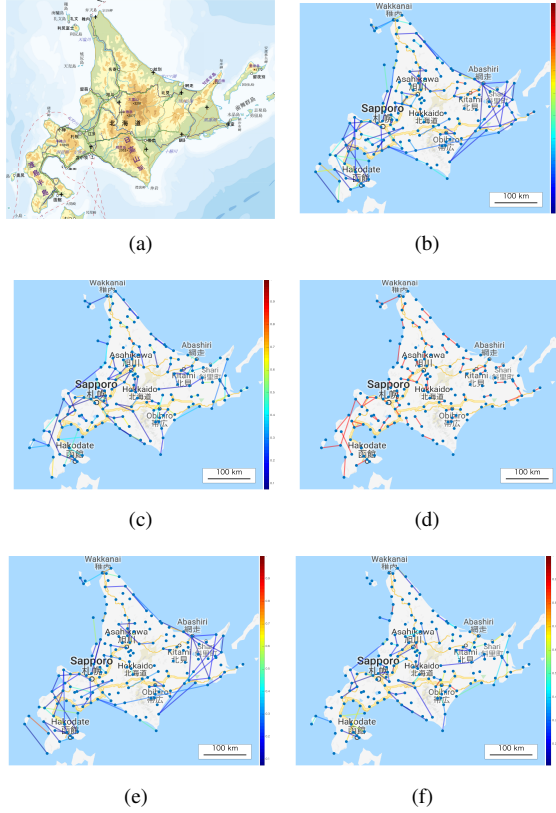


Fig. 6. Visualization of the graph learned from the temperature data. (a) Map of Hokkaido with altitude. (b) Graph learned for January 8, 2015 (winter graph). (c) Graph learned for August 9, 2015 (summer graph). (d) Edges that are common in winter and summer. (e) The winter graph without common edges (winter-specific graph). (f) The summer graph without common edges (summer-specific graph).

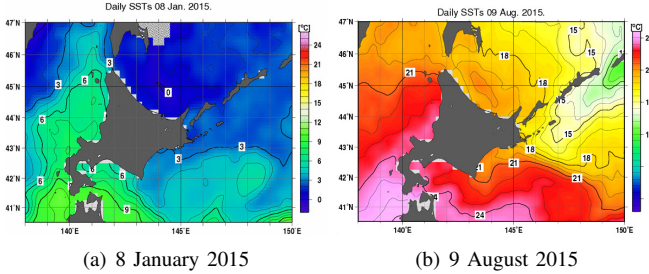


Fig. 7. Daily sea surface temperature in winter (left) and summer (right).

average daily temperature data² collected from 172 locations in Hokkaido in 2015, i.e., the overall dataset has 365 time slots with $N = 172$ and $K = 24$. From this data, we estimate a TV graph by using TGL-TH.

Fig. 6 shows the graph learned from temperature data³. For visualization, we remove edges having very small weight ($< 1.0 \times 10^{-4}$). The learned graph shows that geographically close nodes are generally connected due to similar temperatures, unless separated by features like mountain ranges. Nodes also form connections along the coast—even over long

²The Japan Meteorological Agency provided the daily temperature data from their website at <https://www.jma.go.jp/jma/index.html>

³The Geospatial Information Authority of Japan provided the map in Hokkaido with altitude from their website at <http://www.gsi.go.jp/>

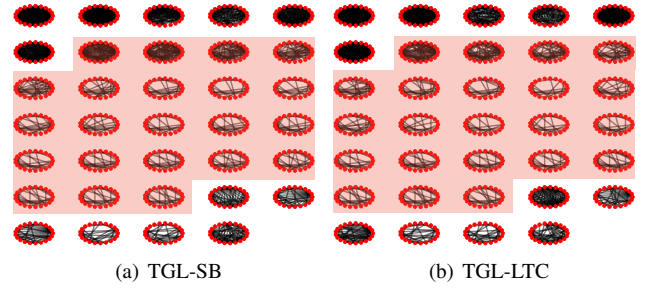


Fig. 8. Brain functional network estimated from bipolar EEG data. The graphs are placed chronologically from left to right, top to bottom. The red areas indicate the graphs during the seizure period. In (a) and (b), we can observe that the network becomes sparse in the middle of the seizure and becomes dense as the seizure ends.

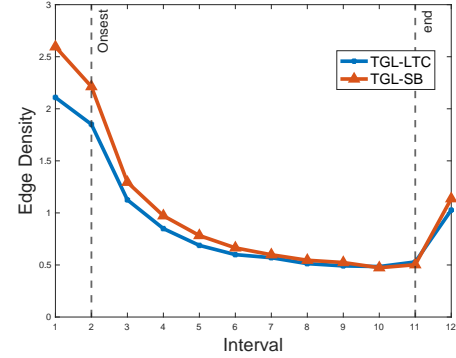


Fig. 9. Average density of graphs for 22 different seizures, estimated with TGL-LTC and TGL-SB. The duration of all seizures is normalized into 12 equal intervals. The interval between two vertical dotted lines reflects the seizure period.

distances—and separately within inland areas. As shown in Fig. 6(d), these local structures remain stable over time.

Figs. 6(e) and 6(f) show the season-specific graphs. We have found that a coastal node often connects to another coastal node, even if they are not close to each other. This can be justified by the warming or cooling effect of sea currents that occur seasonally in this area and affect coastal areas in similar ways. Fig. 7 represents daily sea surface temperatures (SST) on January 8 and August 9, 2015⁴. As can be seen in Figs. 6(e), 6(f), and 7, nodes in similar SST areas are connected to each other in the learned graph. It is important to emphasize that there was no prior information about the SST areas used in the graph learning process.

C. EEG Data

As the last example, we analyzed EEG recordings of epileptic seizures, where brain networks are known to undergo significant topological changes [63]–[65]. We used the CHB-MIT Scalp EEG Dataset [66], focusing on recordings from 125 seconds before seizure onset until its end. Using 5-second non-overlapping windows, we learned TV graphs with TGL-SB and TGL-LTC to track the network evolution during the pre-ictal, ictal, and post-ictal periods. We set the parameters so that the resulting graph is maximally sparse but connected.

⁴The daily SST was provided by Japan Meteorological Agency, from their website at <https://www.jma.go.jp/jma/index.html>

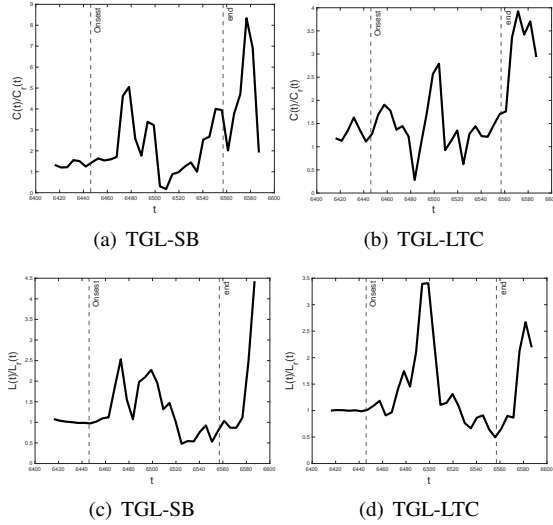


Fig. 10. (a-b) Relative global clustering coefficient and (b-d) relative shortest path length calculated for each graph at time t . The values are smoothed with a 2-point moving average. Dotted lines indicate the onset and end of the seizure.

We first analyze the temporal variation of connectivity by calculating the average edge density for each time window. As shown in Fig. 8 for a representative patient, the learned graphs become sparse during a seizure before gradually recovering as the seizure ends. To confirm this trend, we analyzed 22 seizures from five patients by normalizing the seizure durations into 12 uniform intervals. The average graph density, calculated as $1/N \sum_{i=1}^N d_i$, d_i being the degree of node i , shown in Fig. 9, decreases during the seizure and slightly increases just before it ends. These findings are consistent with previous studies [63], [64].

We further evaluate our results using two small-world network metrics for each t [65]:

- Global clustering coefficient (C_t): a measure for the tendency of nodes to form a cluster, calculated by $C_t = \frac{1}{N} \sum_i c_{i,t}$ where $c_{i,t}$ is the local clustering coefficient defined as $c_{i,t} := 2(|\mathcal{E}_i|)/(k_i(k_i - 1))$ in which \mathcal{E}_i is the number of existing edges in a subgraph of direct neighbors of the i th node and k_i is the number of possible edges within the subgraph.
- Shortest path length (L_t): L_t is the average shortest path between two nodes v_i and v_j , given by $L = \frac{1}{N(N-1)} \sum_{i \neq j} s(v_i, v_j)$ where $s(v_i, v_j)$ is the sum of edge weights in the path.

We calculated the ratios of the clustering coefficient ($C_t/C_{r,t}$) and shortest path length ($L_t/L_{r,t}$) relative to a random ER-graph generated with $p_t = E_t/(N(N-1))$ where E_t is the number of edges in the learned graph at t . Fig. 10 shows these ratios for a representative seizure. We can see that both values tend to peak during a seizure, similar to results in [65], further validating that our methods can capture the functional brain connectivity during epileptic seizures.

VII. CONCLUSION

In this paper, we have presented a framework for learning TV graphs suitable for analyzing spatiotemporal data and

change detection. The framework formulates a TV graph learning problem as a convex optimization problem with constraints on the temporal variation in the graph. Specifically, the framework introduces fused Lasso regularization and group Lasso regularization of the temporal variation to learn the graph having temporal homogeneity, the graph reflecting a sudden change in networks, and one with local topological changes, respectively. We also propose algorithms for solving the optimization problems based on the primal-dual splitting algorithm and extend the algorithm to accommodate multiple memory settings. In synthetic and real data applications, we demonstrated that our proposed model can successfully learn the TV graphs, especially when the number of observations is small.

REFERENCES

- [1] C. Nowzari, V. M. Preciado, and G. J. Pappas, "Analysis and control of epidemics: A survey of spreading processes on complex networks," *IEEE Control Syst. Mag.*, vol. 36, no. 1, pp. 26–46, 2016.
- [2] A. Ganesh, L. Massoulié, and D. Towsley, "The effect of network topology on the spread of epidemics," in *Proc. IEEE INFOCOM*, vol. 2, 2005, pp. 1455–1466 vol. 2.
- [3] V. Colizza, A. Barrat, M. Barthélemy, and A. Vespignani, "The role of the airline transportation network in the prediction and predictability of global epidemics," *The Proceedings of the National Academy of Sciences*, vol. 103, no. 7, pp. 2015–2020, 2006.
- [4] J. Zhang and J. M. F. Moura, "Diffusion in social networks as SIS epidemics: Beyond full mixing and complete graphs," *IEEE J. Sel. Top. Signal Process.*, vol. 8, no. 4, pp. 537–551, 2014.
- [5] N. Shahid, N. Perraudin, V. Kalofolias, G. Puy, and P. Vandergheynst, "Fast robust PCA on graphs," *IEEE J. Sel. Top. Signal Process.*, vol. 10, no. 4, pp. 740–756, 2016.
- [6] F. Shang, L. C. Jiao, and F. Wang, "Graph dual regularization non-negative matrix factorization for co-clustering," *Pattern Recognition*, vol. 45, no. 6, pp. 2237–2250, 2012.
- [7] Z. Zhang and K. Zhao, "Low-rank matrix approximation with manifold regularization," *IEEE Trans. Pattern Anal. Mach. Intell.*, vol. 35, no. 7, pp. 1717–1729, 2013.
- [8] A. Gadde, S. K. Narang, and A. Ortega, "Bilateral filter: Graph spectral interpretation and extensions," in *Proc. IEEE ICIP*, 2013, pp. 1222–1226.
- [9] Y. Wang, A. Ortega, D. Tian, and A. Vetro, "A graph-based joint bilateral approach for depth enhancement," in *Proc. IEEE ICASSP*, 2014, pp. 885–889.
- [10] M. Onuki, S. Ono, M. Yamagishi, and Y. Tanaka, "Graph signal denoising via trilateral filter on graph spectral domain," *IEEE Trans. Signal Inf. Process. Netw.*, vol. 2, no. 2, pp. 137–148, 2016.
- [11] A. Elmoataz, O. Lezoray, and S. Bougleux, "Nonlocal discrete regularization on weighted graphs: A framework for image and manifold processing," *IEEE Trans. Image Process.*, vol. 17, no. 7, pp. 1047–1060, 2008.
- [12] C. Couprie, L. Grady, L. Najman, J. Pesquet, and H. Talbot, "Dual constrained TV-based regularization on graphs," *SIAM J. Imaging Sci.*, vol. 6, no. 3, pp. 1246–1273, 2013.
- [13] S. Ono, I. Yamada, and I. Kumazawa, "Total generalized variation for graph signals," in *Proc. IEEE ICASSP*, 2015, pp. 5456–5460.
- [14] X. Dong, D. Thanou, M. Rabbat, and P. Frossard, "Learning graphs from data: A signal representation perspective," *IEEE Signal Process. Mag.*, vol. 36, no. 3, pp. 44–63, 2019.
- [15] G. Mateos, S. Segarra, A. G. Marques, and A. Ribeiro, "Connecting the dots: Identifying network structure via graph signal processing," *IEEE Signal Process. Mag.*, vol. 36, no. 3, pp. 16–43, 2019.
- [16] G. B. Giannakis, Y. Shen, and G. V. Karanikolas, "Topology identification and learning over graphs: Accounting for nonlinearities and dynamics," *Proc. IEEE*, vol. 106, no. 5, pp. 787–807, 2018.
- [17] S. K. Kadambari and S. Prabhakar Chepuri, "Learning product graphs from multidomain signals," in *Proc. IEEE ICASSP*, 2020, pp. 5665–5669.
- [18] Y. Liu, L. Yang, K. You, W. Guo, and W. Wang, "Graph learning based on spatiotemporal smoothness for time-varying graph signal," *IEEE Access*, vol. 7, pp. 62 372–62 386, 2019.

- [19] M. A. Lodhi and W. U. Bajwa, "Learning product graphs underlying smooth graph signals," *ArXiv*, 2020.
- [20] X. Chen, Y. Liu, H. Liu, and J. G. Carbonell, "Learning spatial-temporal varying graphs with applications to climate data analysis," in *Proc. AAAI Conf. Artif. Intell.* AAAI Press, 2010, pp. 425–430.
- [21] V. Kalofolias, "How to learn a graph from smooth signals," in *Proc. Int. Conf. Artif. Intell. Statist.*, 2016, pp. 920–929.
- [22] X. Dong, D. Thanou, P. Frossard, and P. Vandergheynst, "Learning Laplacian matrix in smooth graph signal representations," *IEEE Trans. Signal Process.*, vol. 64, no. 23, pp. 6160–6173, 2016.
- [23] H. E. Egilmez, E. Pavez, and A. Ortega, "Graph learning from data under Laplacian and structural constraints," *IEEE J. Sel. Top. Signal Process.*, vol. 11, no. 6, pp. 825–841, 2017.
- [24] B. Pasdeloup, V. Gripon, G. Mercier, D. Pastor, and M. G. Rabbat, "Characterization and inference of graph diffusion processes from observations of stationary signals," *IEEE Trans. Signal Inf. Process. Netw.*, vol. 4, no. 3, pp. 481–496, 2018.
- [25] D. Thanou, X. Dong, D. Kressner, and P. Frossard, "Learning heat diffusion graphs," *IEEE Trans. Signal Inf. Process. Netw.*, vol. 3, no. 3, pp. 484–499, 2017.
- [26] J. Mei and J. M. F. Moura, "Signal processing on graphs: Causal modeling of unstructured data," *IEEE Trans. Signal Process.*, vol. 65, no. 8, pp. 2077–2092, 2017.
- [27] S. P. Chepuri, S. Liu, G. Leus, and A. O. Hero, "Learning sparse graphs under smoothness prior," in *Proc. IEEE ICASSP*, 2017, pp. 6508–6512.
- [28] E. Pavez, H. E. Egilmez, and A. Ortega, "Learning graphs with monotone topology properties and multiple connected components," *IEEE Trans. Signal Process.*, vol. 66, no. 9, pp. 2399–2413, 2018.
- [29] H. E. Egilmez, E. Pavez, and A. Ortega, "Graph learning from filtered signals: Graph system and diffusion kernel identification," *IEEE Trans. Signal Inf. Process. Netw.*, pp. 1–1, 2018.
- [30] X. Pu, T. Cao, X. Zhang, X. Dong, and S. Chen, "Learning to learn graph topologies," in *presented at the NeurIPS*, M. Ranzato, A. Beygelzimer, Y. Dauphin, P. Liang, and J. W. Vaughan, Eds., vol. 34. Curran Associates, Inc., 2021, pp. 4249–4262.
- [31] R. Li, J. Lin, H. Qiu, W. Zhang, and J. Wang, "Graph learning for latent-variable Gaussian graphical models under laplacian constraints," *Neurocomputing*, vol. 532, pp. 67–76, 2023.
- [32] A. Tamaru, J. Hara, H. Higashi, Y. Tanaka, and A. Ortega, "Optimizing k in kNN graphs with graph learning perspective," in *Proc. IEEE ICASSP*, 2024, pp. 9441–9445.
- [33] M. G. Preti, T. A. Bolton, and D. Van De Ville, "The dynamic functional connectome: State-of-the-art and perspectives," *NeuroImage*, vol. 160, pp. 41–54, 2017.
- [34] Y. Kim, S. Han, S. Choi, and D. Hwang, "Inference of dynamic networks using time-course Data," *Brief. Bioinformatics*, vol. 15, no. 2, pp. 212–228, 2014.
- [35] D. Hallac, Y. Park, S. Boyd, and J. Leskovec, "Network inference via the time-varying graphical lasso," in *Proc. KDD '17*. Association for Computing Machinery, 2017, pp. 205–213.
- [36] K. Yamada, Y. Tanaka, and A. Ortega, "Time-varying graph learning based on sparseness of temporal variation," in *Proc. IEEE ICASSP*, 2019, pp. 5411–5415.
- [37] V. Kalofolias, A. Loukas, D. Thanou, and P. Frossard, "Learning time varying graphs," in *Proc. IEEE ICASSP*, 2017, pp. 2826–2830.
- [38] X. Zhang and Q. Wang, "Time-varying graph learning under structured temporal priors," in *Proc. EUSIPCO*, 2022, pp. 2141–2145.
- [39] R. Ye, X.-Q. Jiang, H. Feng, J. Wang, R. Qiu, and X. Hou, "Time-varying graph learning from smooth and stationary graph signals with hidden nodes," *EURASIP J. Adv. in Signal Process.*, vol. 2024, no. 1, p. 33, 2024.
- [40] A. Natali, E. Isufi, M. Coutino, and G. Leus, "Learning time-varying graphs from online data," *IEEE Open J. Signal Processing*, vol. 3, pp. 212–228, 2022.
- [41] S. Bagheri, G. Cheung, T. Eadie, and A. Ortega, "Joint signal interpolation / time-varying graph estimation via smoothness and low-rank priors," in *2024 IEEE International Conference on Acoustics, Speech and Signal Processing (ICASSP)*, 2024, pp. 9646–9650.
- [42] S. Saboksayr, S. Aman, G. Mateos, and M. Cetin, "Online discriminative graph learning from multi-class smooth signals," *Signal Processing*, vol. 186, p. 108101, 2021.
- [43] S. Rey, A. Bucileu, M. Navarro, S. Segarra, and A. G. Marques, "Joint inference of multiple graphs with hidden variables from stationary graph signals," in *Proc. IEEE ICASSP*, 2022, pp. 5817–5821.
- [44] R. P. Monti, P. Hellyer, D. Sharp, R. Leech, C. Anagnostopoulos, and G. Montana, "Estimating time-varying brain connectivity networks from functional MRI time series," *NeuroImage*, vol. 103, pp. 427–443, 2014.
- [45] J. Wang, S. Qiu, Y. Xu, Z. Liu, X. Wen, X. Hu, R. Zhang, M. Li, W. Wang, and R. Huang, "Graph theoretical analysis reveals disrupted topological properties of whole brain functional networks in temporal lobe epilepsy," *Clinical Neurophysiology*, vol. 125, no. 9, pp. 1744–1756, 2014.
- [46] R. Velmani and B. Kaarthick, "An efficient cluster-tree based data collection scheme for large mobile wireless sensor networks," *IEEE Sens. J.*, vol. 15, no. 4, pp. 2377–2390, 2015.
- [47] L. Condat, "A primal–dual splitting method for convex optimization involving Lipschitzian, proximable and linear composite terms," *J. Optim. Theory Appl.*, vol. 158, no. 2, pp. 460–479, 2013.
- [48] K. Yamada, Y. Tanaka, and A. Ortega, "Time-varying graph learning with constraints on graph temporal variation," *ArXiv*, 2020.
- [49] D. I. Shuman, S. K. Narang, P. Frossard, A. Ortega, and P. Vandergheynst, "The emerging field of signal processing on graphs: Extending high-dimensional data analysis to networks and other irregular domains," *IEEE Signal Process. Mag.*, vol. 30, no. 3, pp. 83–98, 2013.
- [50] A. Ortega, *Introduction to Graph Signal Processing*. Cambridge University Press, 2022.
- [51] N. Parikh and S. Boyd, "Proximal algorithms," *Found Trends Optim.*, vol. 1, no. 3, pp. 127–239, 2014.
- [52] N. Perraudin and P. Vandergheynst, "Stationary signal processing on graphs," *IEEE Trans. Signal Process.*, vol. 65, no. 13, pp. 3462–3477, 2017.
- [53] R. Tibshirani, M. Saunders, S. Rosset, J. Zhu, and K. Knight, "Sparsity and smoothness via the fused Lasso," *J. R. Stat. Soc. Ser. B Stat. Methodol.*, vol. 67, no. 1, pp. 91–108, 2005.
- [54] Y. Yang, H. T. Shen, Z. Ma, Z. Huang, and X. Zhou, " $\ell_2, 1$ -norm regularized discriminative feature selection for unsupervised learning," in *Proc. IJCAI*, 2011.
- [55] L. Meier, S. V. D. Geer, and P. Bühlmann, "The group Lasso for logistic regression," *J. R. Stat. Soc. Ser. B Stat. Methodol.*, vol. 70, no. 1, pp. 53–71, 2008.
- [56] N. Komodakis and J. Pesquet, "Playing with duality: An overview of recent primal-dual approaches for solving large-scale optimization problems," *IEEE Signal Process. Mag.*, vol. 32, no. 6, pp. 31–54, 2015.
- [57] I. Daubechies, M. Defrise, and C. De Mol, "An iterative thresholding algorithm for linear inverse problems with a sparsity constraint," *Commun. Pure Appl. Math.*, vol. 57, no. 11, pp. 1413–1457, 2004.
- [58] P. Combettes and J. Pesquet, "Primal-dual splitting algorithm for solving inclusions with mixtures of composite, Lipschitzian, and parallel-sum type monotone operators," *Set-Valued and Variational Analysis*, vol. 20, no. 2, pp. 307–330, 2012.
- [59] R. Lambiotte, J.-C. Delvenne, and M. Barahona, "Random walks, markov processes and the multiscale modular organization of complex networks," *IEEE Trans. on Netw. Sci. Eng.*, vol. 1, no. 2, pp. 76–90, 2014.
- [60] D. B. Johnson and D. A. Maltz, "Dynamic source routing in ad hoc wireless networks," in *Mobile Computing*, 1996, pp. 153–181.
- [61] F. Zhang and E. R. Hancock, "Graph spectral image smoothing using the heat kernel," *Pattern Recognition*, vol. 41, no. 11, pp. 3328–3342, 2008.
- [62] J. Gall, C. Stoll, d. E. Aguiar, C. Theobalt, B. Rosenhahn, and H. Seidel, "Motion capture using joint skeleton tracking and surface estimation," in *Proc. IEEE CVPR*, 2009, pp. 1746–1753.
- [63] M. A. Kramer, U. T. Eden, E. D. Kolaczyk, R. Zepeda, E. N. Eskandar, and S. S. Cash, "Coalescence and fragmentation of cortical networks during focal seizures," *J. Neurosci.*, vol. 30, no. 30, pp. 10076–10085, 2010.
- [64] V. E. Diessen, S. J. H. Diederer, K. P. J. Braun, F. E. Jansen, and C. J. Stam, "Functional and structural brain networks in epilepsy: What have we learned?" *Epilepsia*, vol. 54, no. 11, pp. 1855–1865, 2013.
- [65] K. A. Schindler, S. Bialonski, M.-T. Horstmann, C. E. Elger, and K. Lehnertz, "Evolving functional network properties and synchronizability during human epileptic seizures," *Chaos*, vol. 18, no. 3, p. 033119, 2008.
- [66] A. Goldberger, L. , Amaral, L. , Glass, J. Hausdorff, P. Ivanov, R. Mark, J. Mietus, G. Moody, C. Peng, and Stanley, "PhysioBank, PhysioToolkit, and PhysioNet: Components of a new research resource for complex physiologic signals," *Circulation [Online]*, vol. 101, no. 23, pp. e215–e220, 2000.